Supplementary Materials for

Mechano-diffusion of Particles in Stretchable Hydrogels

Chuwei Ye[a]†, Congjie Wei[b]†, Jiabin Liu[a]†, Tsz Hung Wong[a]†, Xinyue Liu[c], Ziyou Song[d], Chenglin Wu[b]*, Zhaojian Li[a]*, Shaoting Lin[a]*

[a] Department of Mechanical Engineering, Michigan State University, East Lansing, MI, USA

[b] Department of Civil and Environmental Engineering, Texas A&M University, College Station, TX, USA

[c] Department of Chemical Engineering and Material Science, Michigan State University, East Lansing, MI, USA

[d] Department of Mechanical Engineering, National University of Singapore, Singapore

†These authors contribute equally to this work: Chuwei Ye, Congjie Wei, Jiabin Liu, Tsz Hung Wong,

*Corresponding authors. Email: chenglinwu@tamu.edu, lizhaoj1@msu.edu, linshaot@msu.edu

This PDF file includes:

Supplementary Text

Materials

Unless otherwise specified, the chemicals used in the current work were purchased from Sigma-Aldrich and used without further purification. For the hydrogels used in the mechano-diffusion experiments, the following materials were used: acrylamide (AAm; Sigma-Aldrich A8887), N, N'-methylenebisacrylamide (MBAA; Sigma-Aldrich 146072), ammonium persulfate (APS; Sigma-Aldrich A3678), N, N, N', N'-tetramethylethylenediamine (TEMED; Sigma-Aldrich T9281), lithium chloride (LiCl; Sigma-Aldrich L9650). The following materials were used in mechano-diffusion experiments under different stress states: acrylic plates (McMaster-Carr), acetic acid (Sigma-Aldrich A6283), 3-(trimethoxysilyl)propyl methacrylate (TMSPMA; Sigma-Aldrich 440159), microscope cover glass (Fisherbrand, Superfrost Plus), and cover glass (Corning). For the gold nanoparticles (AuNPs) synthesis, the following materials were used: deionized water (DI water; Ward's Science 470300-966), gold (III) chloride trihydrate ($HAuCl_4 \cdot 3H_2O$; Sigma-Aldrich 520918), tri-sodium citrate (Sigma-Aldrich S1804) used as stabilization agent, and sodium borohydride ($NaBH_4$; Sigma-Aldrich 452882), methoxypoly (ethylene glycol) 1000-thiol (MPEG1000-SH; Nanosoft Biotechnology SKU 2514-1000), and centrifugal filters (The Amicon Ultra 4 Ultracel 30 kDa molecular weight cutoff; Merck Millipore Ltd.).

Synthesis of functionalized AuNPs

To synthesize AuNPs with precise control over their core and hydrodynamic diameters, we followed a modified protocol [1, 2]. Two kinds of AuNPs with core diameters of 6 nm and 18 nm are synthesized.

Specifically, for the AuNPs with 6 nm core diameter, a mixture of 20 mL DI water, 0.25 mM $HAuCl_4$, and 0.25 mM tri-sodium citrate was stirred magnetically at 650 rpm for 15 minutes (**Fig. S2**). Concurrently, we added 600 μL of ice-cold 0.1 M $NaBH_4$ solution into the mixture, which instantly transformed the initially colorless solution into a vivid red hue. The mixture was left undisturbed for 1 hour to allow the solution to reach the reaction [3]. To enhance the compatibility between the hydrophobic AuNPs and the hydrophilic hydrogel, the AuNPs' surfaces were functionalized with thiol-terminated PEG chains. Specifically, 50 mg of MPEG1000-SH was dissolved in 500 μL of DI water and then added dropwise to the 20 mL AuNPs solution while stirring at 650 rpm, resulting in a solution with deeper color. Subsequently, the mixture was stirred for 1 hour to ensure a thorough ligand exchange. The solution was then allowed to stand for 1 hour to stabilize. Afterward, 4 mL of the solution was transferred to a centrifugal filter and centrifuged at 4000 rpm for 10 minutes to eliminate any residual reagents. This centrifugation process was repeated three times, each time with the addition of 4 mL of DI water. After the final centrifugation, the concentrated AuNPs solution exhibited a dark purple color [4].

For the AuNPs with 18 nm core diameter, a mixture of 20 mL DI water and 0.25 mM $HAuCl_4$ was stirred magnetically at 650 rpm on the hot plate (**Fig. S3**). The hotplate was set at a heating temperature of 180 °C to heat the $HAuCl_4$ solution. When the $HAuCl_4$ solution was boiling, 2 mL of 1% wt. Tri-sodium citrate aqueous solution was slowly added in, and the boiling was continued. The color of the solution first turned light purple and then changed to ruby red after further boiling, indicating the formation of AuNPs. The heating continued for an extra 10 min. The AuNPs solution was cooled down to room temperature. After the cooling process, to enhance the compatibility between the hydrophobic AuNPs and the hydrophilic hydrogel, the AuNPs' surfaces were functionalized with thiol-terminated PEG chains. Specifically, 50 mg of MPEG1000-SH was dissolved in 500 μL of DI water and then added dropwise to the 20 mL AuNPs solution while

stirring at 650 rpm, resulting in a solution with deeper color. Subsequently, the mixture was stirred for 1 hour to ensure a thorough ligand exchange. The solution was then allowed to stand for 1 hour to stabilize. Afterward, this 18 nm AuNPs solution was centrifuged in the same way as that for the 6 nm AuNPs solution.

Structural characterization of AuNPs

The core diameter and hydrodynamic diameter of the AuNPs were characterized by transmission electron microscopy (TEM) imaging and dynamic light scattering (DLS), respectively. Specifically, the TEM imaging was carried out using the JEOL 1400 Flash TEM equipment with a maximum accelerating voltage of 120 kV and a lattice resolution of 0.2 nm; and the DLS was performed using the Malvern Zetasizer Nano-ZS equipment. Given the measured distributions of AuNPs' core diameter and hydrodynamic diameter, we can identify the mean values of core diameter and hydrodynamic diameter of the two kinds of AuNPs as $d_c = 6$ nm and 18 nm (**Fig. S2c, Fig. S3c**) and $d_h = 12$ nm and 28 nm (**Fig. S2d, Fig. S3d**), respectively.

Zeta potential measurement of AuNPs

The zeta potential measurement of the aqueous AuNPs solution was performed by the Malvern Zetasizer Nano-ZS equipment by laser Doppler microelectrophoresis method, using disposable cuvettes with a capillary channel. Both the zeta potential of the AuNPs with 6 nm and 18 nm core diameters were measured (**Fig. S4**). The results show that the conductivities of the solution are 0.335 mS/cm and 0.339 mS/cm. The measured electrophoretic mobilities of the AuNPs with 6 nm core diameter and 18 nm core diameter are -0.07531 μm·cm/V·s and -0.07977 μm·cm/V·s, respectively. By applying Henry's equation and Smoluchowski approximation [5], the zeta potential of the AuNPs samples are -0.961 mV and -1.02 mV. The zeta potential of both AuNPs is nearly 0 mV, indicating that the surface electrokinetic potential of the AuNPs is neutral, and the AuNPs are inert in the aspect of surface charge.

Synthesis of hydrogels

The hydrogel was synthesized for the demonstration of expanded tuning freedom and enlarged tuning degree. Specifically, a 50 mL hydrogel precursor solution was prepared by mixing a 4 M LiCl aqueous solution, 3.5 g of AAm, 30 mg of MBAA, 500 μL of a 10 wt.% APS aqueous solution, and 50 μL of TEMED using a centrifugal mixer (AR-100, THINKY). The introduction of the LiCl salt served the purpose of preventing significant dehydration during prolonged diffusion experiments (**Fig. S5**). Subsequently, the hydrogel precursor solutions were subsequently cured in an acrylic mold which was cut using a laser cutter (EpilogLaser) and assembled using superglue (Krazy). The hydrogel precursor solution was then poured into the mold with the cuboid securely positioned at the top to form a reservoir. The assembly was subsequently placed in an oven (CL-1000 Ultraviolet Crosslinker) and cured at 60 °C for 2 hours. Afterward, the concentrated AuNPs were injected into the central reservoir for further measurement and analysis.

Identification of hydrogel mesh size

With the assumption that hydrogel is fully swollen and water is a good solvent, the distance between neighboring crosslinkers at the undeformed state R_0 can be estimated by the following relationship [6],

$$R_0 \sim a\phi^{-0.75}C_\infty^{-0.25}(1-2\chi)^{-0.25} \quad \text{(S1)}$$

where a = 0.154 nm is the equivalent bond length of AAm monomer, ϕ is the volume fraction as 3% for the hydrogel, $C_\infty = 15.2$ is the characteristic ratio of PAAm polymer, and $\chi = 0.466$ is the Flory interaction parameter between PAAm polymer and water molecules.

Construction of customized mechano-diffusion characterization platform

Figure S1 illustrates the schematics of the customized mechano-diffusion characterization platform. The platform can be divided into the mechanical loading module, the force/torque measurement module, and the imaging module. In the mechanical loading module, a two-phase stepper motor drives a 1604-type ball screw with a linear guide to achieve static or dynamic uniaxial stretching of the hydrogel samples. Additionally, another two-phase stepper motor is used to apply torsion loads to the hydrogel samples. An Arduino UNO microcontroller controls the movement of this module. The force/torque measurement module integrates a force sensor with a 9.8 N measurement range and a 1.9 mV/V sensitivity, as well as a torque sensor with a 0.3 Nm measurement range and a 0.6 mV/V sensitivity. Since the sensor outputs are at millivolt levels, an amplification circuit based on an INA128P instrumental amplifier amplifies the signals to volt levels. These measured forces and torques are then calculated and recorded on a computer via an NI USB 6008 data acquisition board and LabVIEW software. In the imaging module, a high-resolution camera with a maximum resolution of 3264 × 2448 pixels and a video capture capability of 15 frames per second captures images. This setup depicts the diffusion profiles of the AuNPs in the hydrogel. During experiments, the camera's spatial resolution is approximately 0.015 mm/pixel, which is sufficient for determining diffusivity, as the diffusion profiles are at the millimeter scale.

Characterization of mechano-diffusion under uniaxial tension and torsion

Figure S6a illustrates the experimental setup of the mechano-diffusion characterization under uniaxial tension and torsion, which consists of a mechanical system for applying the uniaxial tensile deformation and an imaging system for recording the diffusion process of AuNPs along the radial direction. The mechanical system involves a cylindrical hydrogel confined by two glass slides. The hydrogel was covalently bonded to the glass slides, following our previously reported protocol [7] (**Fig. S6b**). Specifically, we prepared a silane solution by vigorous magnetic stirring (300 rpm) a mixture of 200 mL of DI water, 30 μL of acetic acid, and 800 μL of TMSPMA for 2 hours until the mixture became transparent. Subsequently, the glass slides were submerged in the solution for 1 hour, resulting in the functionalization of hydroxyl groups on the glass surface with silane TMSPMA via covalent siloxane chemistry. The covalent bonding between the functionalized glass and the hydrogel were achieved through the polymerization of the precursor solution onto the glass slides.

For the sample under uniaxial tension, the lower glass (**Fig. S6a**) is fixed while the upper glass is lifted so that the cylindrical hydrogel sample is stretched along its axial direction with specific stretch ratios. Then, the AuNPs solution is dropped into the center vacancy of the hydrogel sample (**Fig. S6a**). The radial diffusion profile of the AuNPs in the hydrogel is observed under the undeformed state every 30 min from a camera placed under the lower glass, and the total diffusion time for each sample is 150 min.

For the sample under torsion, the lower glass is fixed while the upper glass is rotated so that a twisting angle is formed between the upper and lower surfaces of the hydrogel sample. Then, the AuNPs solution is dropped into the center vacancy of the hydrogel sample (**Fig. S6a**). The radial diffusion profile of the AuNPs in the hydrogel is observed under the undeformed state every 30

min from a camera placed under the lower glass, and the total diffusion time for each sample is 150 min.

To estimate the diffusivity of the AuNPs in the hydrogel medium, we implement the following method to rigorously analyze the spatiotemporal concentration distribution of the AuNPs in the diffusion process.

The 1D governing diffusion equation in the Cartesian coordinate system is as follows:

$$\frac{\partial c}{\partial t} = D\frac{\partial^2 c}{\partial x^2} \tag{S2}$$

where c is concentration, t is diffusion time, x is diffusion distance, and D is diffusivity. In the cylindrical coordinate system, Eq. (S2) can be further expressed as:

$$\frac{\partial c}{\partial t} = D\left(\frac{1}{r}\frac{\partial}{\partial r}\left(r\frac{\partial c}{\partial r}\right) + \frac{1}{r^2}\frac{\partial^2 c}{\partial \theta^2} + \frac{\partial^2 c}{\partial z^2}\right) \tag{S3}$$

where r is the diffusion distance along the radial direction, z is the axial distance, θ is the angular coordinate. Since the diffusion is symmetrical in the angular direction, namely $\partial c/\partial\theta = 0$, the Eq. S3 can be further simplified as:

$$\frac{\partial c}{\partial t} = D\left(\frac{1}{r}\frac{\partial}{\partial r}\left(r\frac{\partial c}{\partial r}\right) + \frac{\partial^2 c}{\partial z^2}\right) = D\left(\frac{\partial^2 c}{\partial r^2} + \frac{1}{r}\frac{\partial c}{\partial r} + \frac{\partial^2 c}{\partial z^2}\right) \tag{S4}$$

In this study, the cylindrical sample occupies the domain where $-9 < r < 9$ and $0 < z < 6$ in millimeters (mm) as illustrated in **Fig. S7a**. The concentration of AuNPs in the reservoir that occupies the domain where $-1.5 < r < 1.5$ and $3 < z < 6$ is set as a constant $c = c_0$, and the initial concentration in the rest of the sample is set as $c = 0$. We use the finite difference methods in MATLAB to numerically solve Eq. S4. We can determine the measured diffusivity D by fitting the simulated concentration profile to the measured concentration profile.

Characterization of mechano-diffusion under biaxial tension

Figure S12a illustrates the experimental setup of the mechano-transport characterization under biaxial tension, which consists of a mechanical system for applying *x*-*y* plane biaxial tensile deformation and an imaging system for recording the diffusion process of AuNPs along the *z* direction. The four side surfaces of the cubic hydrogel sample are bonded with the glass slides via the glass-bonding technique according to the existing protocol [7]. The four sides of the hydrogel sample can be stretched by moving the glass slides in *x* and *y* directions. The AuNPs solution is injected into the vacancy of the cubic hydrogel sample, and the diffusion profile along the *z* direction is observed by a camera. The total diffusion time is 240 min (**Fig. S12b**).

To estimate the diffusivity of the AuNPs in the hydrogel medium, we implement the following method to rigorously analyze the spatiotemporal concentration distribution of the AuNPs in the diffusion process.

The 3D governing diffusion equation in the Cartesian coordinate system is as follows:

$$\frac{\partial c}{\partial t} = D\left(\frac{\partial^2 c}{\partial x^2} + \frac{\partial^2 c}{\partial y^2} + \frac{\partial^2 c}{\partial z^2}\right) \quad (S5)$$

where c is concentration, t is diffusion time, x, y, and z are diffusion distance, and D is diffusivity. In this case, the concentration distribution along the z direction is under observation since the x and y directions of the hydrogel sample are under tension loads.

In this study, the cubic sample occupies the domain where $-10 < x < 10$, $-10 < y < 10$, and $0 < z < 20$ in millimeters (mm) as illustrated in **Fig S13**. The concentration of AuNPs in the reservoir that occupies the domain where $-1.5 < x < 1.5$, $-1.5 < y < 1.5$, and $10 < z < 20$ is set as a constant $c = c_0$, and the initial concentration in the rest of the sample is set as $c = 0$. We use the finite difference methods in MATLAB to numerically solve Eq. S5. We can determine the measured diffusivity D by fitting the simulated concentration profile to the measured concentration profile.

Coarse-grained molecular dynamics simulation

The coarse-grained (CG) molecular dynamics (MD) modeling is based on the molecular dynamic simulation software package LAMMPS. The simulation flow chart is illustrated in **Fig. S15**. A 3D crosslinked network is constructed with 3546 sphere monomers that are modeled with CG beads. To model the influence of the solutions on the diffusion mechanism, solution CG beads are also constructed with an initial uniform interval of 1σ along all directions. Using the Lennard-Jones (LJ) unit system, the diameter of the CG bead σ for the polymer chains was set as the length unit, while the diameter for the solution CG beads was set as 0.1σ. Along all three directions, the length of polymer chains is set as 36σ while the periodic boundary conditions (PBC) are applied. Cubic cells with a uniform side length of 6σ are considered, creating 8 polymer chains along each direction and a total of 125 cells in the whole system via the crosslinkers. Nanoparticles are initially located in the middle.

LJ potential is used to represent the long-term interactions between the monomers of both polymer chains as well as solution and nanoparticles as well as in between monomers with the following equation [8],

$$U_{ij} = 4\varepsilon\left(\left(\frac{r_0}{r}\right)^{12} - \left(\frac{r_0}{r}\right)^{6}\right) \quad (S6)$$

where r is the distance between each pair of CG beads and r_0 is the characterized length parameter and set as $r_0 = 1\sigma$ for the interactions between monomers and $r_0 = 3\sigma$ for the interactions between monomers and nanoparticles. The overall cut-off radius was set as 2.5σ for all setups to define the largest interactive distance between all CG beads. $\varepsilon = 0.1kT$ is the interaction parameter set for the monomer interactions, where k is the Boltzmann constant and $T = 0.01$ is the system temperature. Other than the LJ potential, adjacent monomers within the polymer system are also defined with 2-body bond connections and 3-body angle restrictions, which are assumed to follow the harmonic bond potential,

$$U_b = k_b(r - r_0)^2 \quad (S7)$$

where $k_b = 25kT/\sigma^2$ is a constant and r_0 is the characterized length parameter representing the stable distance with 0 force. The r is the real-time distance between bonded CG beads.

The CG motion is governed by the Langevin equation [9],

$$\frac{dr_i}{dt} = \frac{1}{\gamma_i} F_i + \sqrt{\frac{2kT}{\gamma_i}}\, f_i(t) \qquad (S8)$$

where F_i is the total force applied to the system, γ_i is the friction coefficient, t is the time, and $f_i(t) \sim N(0,\ \sigma)$ is the random force that follows the normal distribution and satisfies

$$\langle f_i^{\alpha}(t) \rangle = 0\ \&\ \langle f_i^{\alpha}(t) f_j^{\beta}(t') \rangle = \delta_{ij}\delta_{\alpha\beta}\delta(t - t') \qquad (S9)$$

where α, β denote the spatial dimensions and δ is the Kronecker delta.

The parameter setups referred to this work [8]. The tensile behavior of one single-string polymer chain is first studied with former setups. As shown in **Fig. 5A**, a polymer chain with 6 monomer CG beads is first constructed and stabilized to achieve the structure file at a relaxed state.

In the modeling of the uniaxial stretching process, the stabilization is first conducted with NVT ensemble for a total 1×10^6 steps. The time step is set as 0.0001τ where $\tau = \sigma\sqrt{m/\varepsilon}$ is the time unit of the LJ unit system. Afterward, the left end monomer is totally fixed along all 3 directions while the right end monomer is moved at a constant velocity of 0.1 σ/τ for a total 2.4×10^6 steps. For the hopping diffusion modeling cases, the model constructed as shown in **Fig. 5A.** is used. After equilibrium using the same setups as the uniaxial stretching case, the atoms around the cell boundaries are fixed along all directions for consideration of stabilization and the whole system is equilibrated under NVT ensemble for a total 5×10^6 steps. The trace of the nanoparticle is recorded, and the diffusivity is represented with

$$D = \lim_{t \to \infty} \left(\frac{MSD}{6t} \right) \qquad (S10)$$

where *MSD* is the time-averaged mean square displacements defined by

$$MSD = \langle \left(r(t_0 + t) - r(t_0) \right)^2 \rangle \qquad (S11)$$

To study the influence of the nanoparticle diameter on the diffusivity, cases with different nanoparticle sizes (ranging from nanoparticle diameter $d = 0$ to $d = 2R_0$, where $R_0 = 6\sigma$ is the mesh size ξ) are constructed and modeled. It should be noted that the density of the polymer and solution CG particles are all set as 1.0. As for the particle, the density is also set as 1.0 for cases with a diameter of 1.0. To remain consistent, the total weight of the particle is set to be the same for all particles of different diameters while the density is adjusted accordingly.

Following the same modeling procedure and setup, we next studied the diffusivity of nanoparticles within the biaxial stretched polymer networks. We modeled the cases with the polymer network was stretched along *x* and *y* directions with a stretch ratio of λ ranging from 1.0 to 4.0. The normalized diffusivity with respect to the value within undeformed polymer chains ($\lambda = 1.0$) is used for the comparison. It should be noted that the total number of polymer and solution CG beads are reduced without losing the comparability with the undeformed case. As shown in **Fig. 5 F-H**, when the particle size is much smaller or much larger than the cell size ($d = 0.5\xi$ or $d = 6.0\xi$), the diffusivity will not be influenced by the deformation ratio. In the former case, the

particle is nearly free to move along all directions while in the latter case, the particle is constrained in the cell where it was initially placed into. As for the case with medium particle size ($d = 4.0\xi$), with the cell size increasing, the diffusivity increases significantly.

Fabrication of pressure-triggered drug delivery system

The pressure-triggered drug delivery system consists of a closed-loop pneumatic actuator and a drug-load hydrogel membrane. The closed-loop pneumatic actuator consists of a chamber made from high-stiffness silicon rubber, sealed by a deformable membrane made from low-stiffness rubber, and a closed-loop control system. The combination of the high-stiffness silicon chamber and the low-stiffness membrane is fabricated via the lost-wax method (**Fig. S18**) [10]. We first cured a wax cylinder as a sacrificial support in an acrylic mold. Subsequently, a high-stiffness silicon rubber (Smooth SIL-940) precursor solution was poured into the mold to form a stiff hollow chamber measuring 45 mm × 50 mm (inner diameter × height), followed by the addition of a low-stiffness silicon rubber (Eco flex 00-20) to form a 2-mm deformable membrane. After an overnight curing, the entire assembly was submerged into a hot water bath at 80 ℃ for melting the wax cylinder, yielding the pneumatic actuator. We also developed a closed-loop control system to regulate the pressure of the actuator (**Fig. S19**), which comprised components including a microcontroller (Arduino UNO), a motor driver board (L298N), an air pump, a pressure sensor (MPX10GP-ND), and the elastomeric actuator. The pressure sensor monitors the pressure within the inflated actuator and transmits the pressure as feedback to the microcontroller. Based on the feedback pressure, the microcontroller makes real-time adjustments to the speed of the air pump by manipulating the duty cycle of the pulse width modulation (PWM) output set to the monitor driver board. This closed-loop control mechanism enables precise and consistent pressure settings within the pneumatic actuator, ensuring a stable deformation applied on the drug-loaded hydrogel. To covalently bond a drug-loaded hydrogel onto the deformable membrane, we adopted the benzophenone-induced grafting photopolymerization [11]. The pristine silicon membrane was first thoroughly cleaned with ethanol and deionized water, and completely dried with nitrogen gas. Thereafter, 200 μL of 10 wt% benzophenone solution was smeared evenly onto the membrane for 10 min at room temperature. The benzophenone-treated membrane was further immersed in a drug-loaded hydrogel precursor solution, subjected to ultraviolet irradiation in an ultraviolet chamber (365 nm ultraviolet; UVP CL-1000) for 30 minutes. The hydrogel precursor solution was prepared by mixing aqueous solutions of 10 mL 12 wt% AAm as the monomer, 1 mL 0.23 wt% MBAA as the crosslinker, 200 μL APS as the initiator, 10 μL TEMED as the accelerator, and 500 μL concentrated AuNPs solution. Under UV radiation, the monomers form PAAm polymers via free radical polymerization; meanwhile, surface absorbed benzophenone mediates the grafting of PAAm polymers onto the reactive sites at the surface of the silicon rubber.

Supplementary Text

1. Particle diffusion in liquid medium

Particle diffusivity D in liquid medium is typically governed by medium viscosity η following the Einstein-Stokes equation $D = (k_B T)/(3\pi\eta d)$, where k_B is the Boltzmann constant, T is the absolute temperature in Kevin, and d is the particle diameter [12, 13]. The viscosity of liquid medium strongly depends on temperature. Here, we choose water, diluted polymer solution, and concentrated polymer solution as representative liquid medium to illustrate their capabilities of tuning particle diffusivity via temperature variation. Given the temperature-dependent viscosity of water $\eta = A\exp\left(\frac{B}{T} + CT + DT^2\right)$ [14], the particle diffusivity tuning ratio by temperature variation from 273 K to 333 K in water can be calculated via

$$\frac{D}{D_0} = \frac{T\eta_0}{AT_0\exp\left(\frac{B}{T} + CT + DT^2\right)} \tag{S12}$$

where $A = 1.856 \times 10^{-11}$ mPa · s, $B = 4209$ K, $C = 0.04527$ K^{-1}, $D = -3.376 \times 10^{-5}$ K^{-2}, D_0 and η_0 are particle diffusivity and viscosity of water at reference temperature T_0. Given the temperature-dependent viscosity of polymer solution $\eta \sim T^{-m}$ [15], the particle diffusivity tuning ratio by temperature variation from 273 K to 333 K in polymer solution can be calculated via

$$\frac{D}{D_0} = \left(\frac{T}{T_0}\right)^{1+m} \tag{S13}$$

where m is the exponent equal to 0.5 for diluted polymer solution [16] and 9 for concentrated polymer solution [15, 17, 18], D_0 and η_0 are particle diffusivity and viscosity of polymer solution at reference temperature T_0. Figure S1A plots the particle diffusivity tuning by temperature variation from 273 K to 333K in water, diluted polymer solution (DPS), and concentrated polymer solution (CPS) with $T_0 = 293$ K.

2. Particle diffusion in porous medium

Particle diffusivity tuning by mechanical deformation in porous medium is mainly attributed to the deformation-induced changes in porosity. The strain-dependent particle diffusivity in porous medium can be described via

$$\frac{D}{D_0} = \frac{\mathrm{e}^J - 1}{\mathrm{e} - 1} \tag{S14}$$

where J is the volumetric Jacobian, D_0 is the particle diffusivity in porous medium at undeformed state [19]. Specifically, when the porous medium is subject to uniaxial tensile deformation, $J = 1 + (\lambda - 1)(1 - 2\nu)$ with λ being the uniaxial stretch and ν being the Poisson's ratio. **Figure S11b** plots the particle diffusivity tuning by uniaxial deformation in porous medium with various Poisson's ratio.

3. Particle diffusion in the undeformed polymeric medium

The mode of particle diffusion in the undeformed polymeric medium is governed by particle size d. When particle size d is smaller than the monomer radius r_f ($d < r_f$), the mode of particle diffusion is dominated by the Einstein-Stokes equation [12, 13], expressed as

$$D_{sol} = \frac{k_B T}{3\pi\eta d} \tag{S15}$$

where η is the viscosity of liquid solvent surrounding the polymeric medium. When particle size d is larger than the monomer radius r_f while smaller than the mesh size ξ ($r_f < d < \xi$), the mode of particle diffusion is dominated by the Obstacle model [20], expressed as

$$\frac{D}{D_{sol}} = \exp\left[-\frac{\pi}{4}\left(\frac{d + 2r_f}{\xi + 2r_f}\right)^2\right] \tag{S16}$$

When particle size d is comparable to or larger than the mesh size ξ, the mode of particle diffusion is dominated by the Hopping diffusion model [21], expressed as

$$D \cong \frac{\xi_c^2}{\tau_x}\left(\frac{d}{\xi}\right)^{-1} \exp\left(-\left(\frac{d}{\xi}\right)^2\right) \tag{S17}$$

where ξ_c is the correlation length of the polymer, and τ_x is the relaxation time of a network.

4. Particle diffusion in the deformed polymeric medium

In this work, we formulate a cross-scale mechano-transport theory to establish the relationship between macroscopic large deformation of bulk materials and microscale hopping diffusion of particles by integrating three models (**Fig. S14**): 1) eight-chain model to relate the macroscopic bulk deformation to the deformation of an individual polymer chain [22], 2) ideal chain model to correlate the free energy of an individual polymer chain with the polymer chain deformation [23], and 3) hopping diffusion model to relate the particle diffusivity to the energy barrier experienced by particles [21, 24].

4.1 Eight-chain model

Following the Arruda-Boyce model [22], the bulk material can be envisioned as an eight-chain network system, considering eight orientations of chains in space within a representative unit cube. The cube edges are taken to remain aligned with principle stretch space during deformation while chains linked at the center of the tube extend to the eight corners. By assuming the bulk material follows the standard kinematics of finite strain deformation, the chain length R is correlated with the principle stretches λ_1, λ_2, λ_3 imposed on the bulk material,

$$\Lambda = \sqrt{\frac{(\lambda_1^2 + \lambda_2^2 + \lambda_3^2)}{3}} \tag{S18 - 1}$$

where $\Lambda = R/R_0$ is the chain stretch with R being the chain length in the current state and R_0 being the chain length in the undeformed state. Equivalently, Eq. (S14-1) can be rewritten as

$$\Lambda = \sqrt{\frac{\mathrm{tr}(\mathbf{F}^{\mathrm{T}}\mathbf{F})}{3}} \qquad (S18-2)$$

where **F** is the deformation gradient of the bulk material.

4.2 Ideal chain model

Following the Langevin chain statistics [23], the individual polymer chain can be envisioned as a freely rotating chain segment consisting of *N* rigid links of equal length *b*. The initial chain length can be calculated based on a random walk statistical analysis,

$$R_0 = \sqrt{N}b \qquad (S19)$$

Notably, the initial chain length determines the mesh size of the polymer network, namely $R_0 = \xi$. When the freely jointed chain is subjected to a constant elongation force f, the chain length in the current state R corresponds to the given force f via a Langevin dependence following,

$$f = \frac{k_B T}{b}\mathcal{L}^{-1}\left(\frac{R}{Nb}\right) \qquad (S20)$$

where $\mathcal{L}^{-1}(x)$ is the inverse Langevin function defined by $\mathcal{L}(x) = \coth(x) - 1/x$. The free energy of an individual polymer chain can be further calculated by $E_e = \int_{R_0}^{R} f dR$, expressed as

$$E_e = N k_B T\left(\frac{\beta}{\tanh\beta} + \ln\frac{\beta}{\sinh\beta}\right) \qquad (S21)$$

where $\beta = \mathcal{L}^{-1}(\Lambda/\sqrt{N})$.

4.3 Hopping diffusion model.

Hopping diffusion refers to a mechanism of nanoparticle movement within polymer networks as they transport through the polymer network by intermittently hopping from one location to another. Different from the particle diffusion governed by Einstein-Stokes equation, particle diffusivity in polymer networks is governed by the elastic energy barrier *U* that is experienced by polymer chains interacting with nanoparticles during their movement. Following the Cai-Rubinstein model [21], the hopping particle diffusivity can be approximated as

$$D \cong \frac{\xi_c^2}{\tau_x}\left(\sqrt{\frac{U}{k_B T}}\right)^{-1} \exp\left(-\frac{U}{k_B T}\right) \qquad (S22)$$

where ξ_c is the correlation length, which can be replaced by the Kuhn length b in unentangled polymer networks as the hopping step size, and $\tau_x \cong \tau_0 N$ is the Rouse relaxation time of the polymer network with τ_0 being the relaxation time of monomers and N being the number of Kuhn monomers. When particles diffuse in the same polymer network at undeformed and deformed states, the particle diffusivity tuning ratio can be calculated by

$$\frac{D}{D_0} \cong \sqrt{\frac{U_0}{U}} \exp\left(-\frac{U-U_0}{k_B T}\right) \tag{S23}$$

where D_0 and U_0 are particle diffusivity and corresponding energy barrier in the undeformed polymer network.

4.4 Case study: Impact of Equal Biaxial Tensile Loading on Particle Diffusivity

In this section, we employ the mechano-transport theory [25] to investigate the mechanism of particle diffusion in biaxially stretched hydrogels. The mechano-transport theory is used to establish the relationship between the macroscopic deformation of soft materials and the microscopic diffusion of particles. It integrates three models: the eight-chain model [23, 26], which relates the bulk deformation of the material to the stretch state of individual chains; the polymer chain model [27], which calculates the energy required to stretch these chains; and diffusion models [20, 21], which quantifies the diffusivity of particles across different diameters.

When the hydrogel undergoes mechanical deformation, according to the eight-chain theory, each polymer chain is stretched with an identical stretch ratio Λ, which is expressed as

$$\Lambda = \sqrt{\frac{1}{3}(\lambda_1^2 + \lambda_2^2 + \lambda_3^2)} \tag{S24}$$

where λ_1, λ_2, λ_3 are three principal stretch ratios imposed on the bulk material. When the hydrogel is subjected to the biaxial tension with stretch ratio λ, the three principal stretch ratios are $\lambda_1 = \lambda_2 = \lambda$, $\lambda_3 = \frac{1}{\lambda^2}$. Following Eq. (S24), the stretch ratio of an individual polymer chain Λ when subjected to biaxial tension can be expressed as a function of the stretch ratio λ

$$\Lambda = \sqrt{\frac{1}{3}\left(2\lambda^2 + \frac{1}{\lambda^4}\right)} \tag{S25}$$

From **Fig. S17b**, the stretch ratio of an individual polymer chain Λ increases with stretch ratio λ.

To quantify the diffusivity of particles in the polymeric medium, we adopted two diffusion models: the obstruction model [20] for small particles and the hopping diffusion model [21] for large particles. For particles smaller than the material's mesh size, the movement of particles is restricted by encountering a series of polymer chains that act as obstacles, leading to a reduction in particle diffusivity when compared with pure liquid medium. The obstruction model considers the probability of particles encountering obstacles to express the particle diffusivity in a polymeric gel D_0 normalized by the liquid diffusivity of its corresponding solvent D_{liq}, as follows

$$\frac{D_0}{D_{liq}} = \exp\left[-\frac{\pi}{4}\left(\frac{d}{\xi}\right)^2\right] \tag{S26}$$

Where d is particle diameter, ξ is the mesh size of polymer network. The particle diffusivity decreases with the increase of the particle size. When the hydrogel is subjected to biaxial tension along *x*, *y* direction with stretch ratio λ, the mesh size along z direction is expanded with a ratio λ. Applying Eq. (S26), the particle diffusivity ratio D/D_0 is expressed as

$$\frac{D}{D_0} = \exp\left[-\frac{\pi}{4}\left(\frac{1}{\lambda^2} - 1\right)\frac{d^2}{\xi^2}\right] \quad (S27)$$

where D is the particle diffusivity at deformed state and D_0 is the particle diffusivity at undeformed state. The diffusivity, as depicted in **Fig. 4E**, shows a monotonic increase until it reaches a plateau with the rise in the biaxial stretch ratio. The enhancement of diffusivity (D/D_0) of larger particle (e.g., $d/\xi = 0.5$) is more pronounced for small particles (e.g., $d/\xi = 0.1$).

For particles larger than polymer's mesh size, the particles need to overcome an energy barrier to transit from one confined cage to an adjacent one. According to the hopping diffusion model, the particle diffusivity in an undeformed polymer network can be approximated as follows:

$$D \cong \frac{\xi_c^2}{\tau_x}\left(\sqrt{\frac{U}{k_B T}}\right)^{-1} \exp\left(-\frac{U}{k_B T}\right) \quad (S28)$$

where U is the energy barrier, k_B is the Boltzmann constant, T is the temperature in Kelvin, ξ_c is the correlation length of polymer network and τ_x is the relaxation time of the polymer network. The energy barrier U is determined by the difference in free energy of the polymer chains under different stretch states:$U = \mathrm{W}(\Lambda_H) - \mathrm{W}(\Lambda_L)$, where Λ_H represents the higher stretch state, Λ_L represents the lower stretch state. Following Eq. (S28), when particles diffuse within the same material system, the ratio of diffusivity in the deformed state D to that in the undeformed state D_0 can be quantified by comparing the energy barriers required in these two states:

$$\frac{D_1}{D_0} = \sqrt{\frac{U_0}{U_1}}\exp\left(\frac{U_0 - U_1}{k_B T}\right) \quad (S29)$$

where U_0 is the energy barrier need to overcome at undeformed polymer network, and U_1 is the energy barrier for deformed polymer network. As shown in **Fig. 4D**, when biaxial tension is applied in the *x* and *y* directions, the polymer chains must stretch to form a square cage with a length equal to the particle diameter if the particles move through the polymer network in the *z* direction. For large particle diffuse through polymer network at undeformed state, the higher stretched state Λ_{H_0} is

$$\Lambda_{H_0} = \sqrt{\left(\frac{d}{\xi}\right)^2 + \frac{1}{3}} \quad (S30)$$

The energy barrier at undeformed polymer network is $U_0 = W(\Lambda_{H_0})$. For large particles diffusing through a biaxially deformed polymer network, since each polymer chain has been stretched by the biaxial tension the lower stretch state $\Lambda_L = \sqrt{\frac{1}{3}(2\lambda^2 + \frac{1}{\lambda^4})}$. The higher stretch state is

$$\Lambda_H = \sqrt{\left(\frac{d}{\xi}\right)^2 + \frac{1}{3\lambda^4}} \quad (S31)$$

The energy barrier at biaxial stretched polymer network is $U_1 = W(\Lambda_H) - W(\Lambda_L)$. Following Eq. (S29), the diffusivity ratio between deformed and undeformed state is

$$\frac{D_1}{D_0} = \sqrt{\frac{W(\Lambda_{H_0})}{W(\Lambda_H) - W(\Lambda_L)}} \exp\left(\frac{W(\Lambda_{H_0}) - W(\Lambda_H) + W(\Lambda_L)}{k_B T}\right) \quad (S32)$$

Based on Eq. (S32), the diffusivity ratio is not only related with the ratio between particle size and mesh size d/ξ, but also is a function of biaxial stretch ratio λ. Additionally, the diffusivity ratio is determined by the free energy of individual polymer chains, which is calculated by integrating the displacement-force relationship $W = \int_1^{\lambda} F ds$, where s is the displacement, F represents the displacement-force relationship, and λ represents the stretched level of individual polymer chain. To quantify the diffusivity ratio, we utilize the force-displacement curve, consistent with the results from MD simulations, as shown in **Fig. S17c**. **Fig. S17d-f** illustrates the relationship between the diffusivity ratio and the biaxial stretch ratio for various particle sizes. As the biaxial stretch ratio increases, the diffusivity ratio rises. This enhancement in diffusivity is particularly significant for larger particles (e.g., d/ξ = 4), as the biaxial stretch in the bulk material greatly reduces the energy barrier.

Fig. S1.

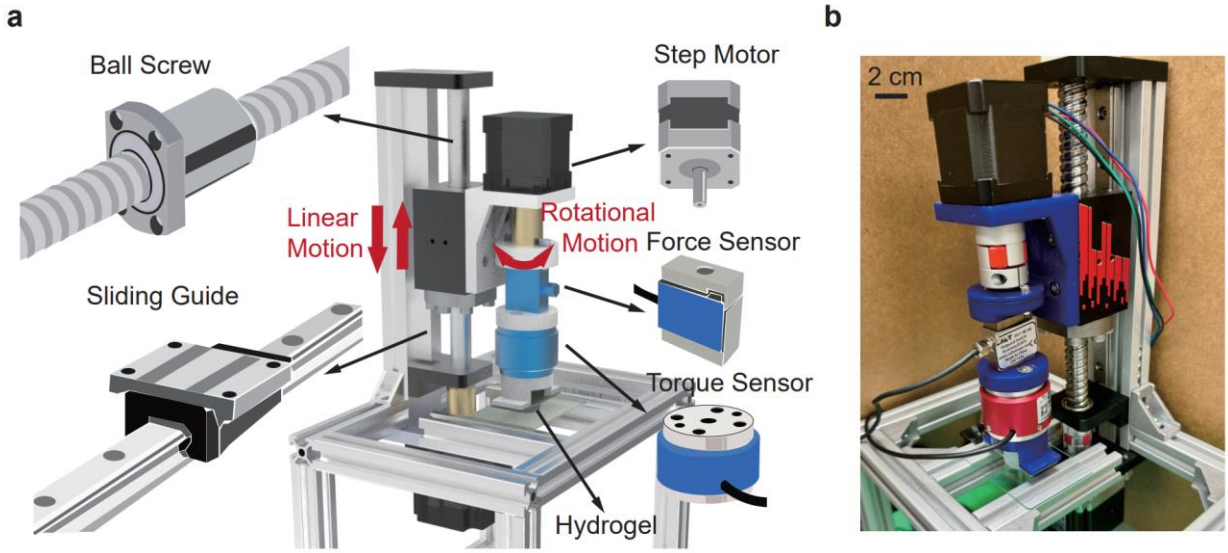

Mechanical system of the customized mechano-diffusion characterization platform. a, Schematic illustration and **b**, optical image of the mechanical platform to apply controlled tension and torsion loads to hydrogels, which consists of a linear motion slide and step motor as the driver, a force sensor to measure the applied force, and a torque sensor to measure the applied torque. The scale bar is 2 cm.

Fig. S2.

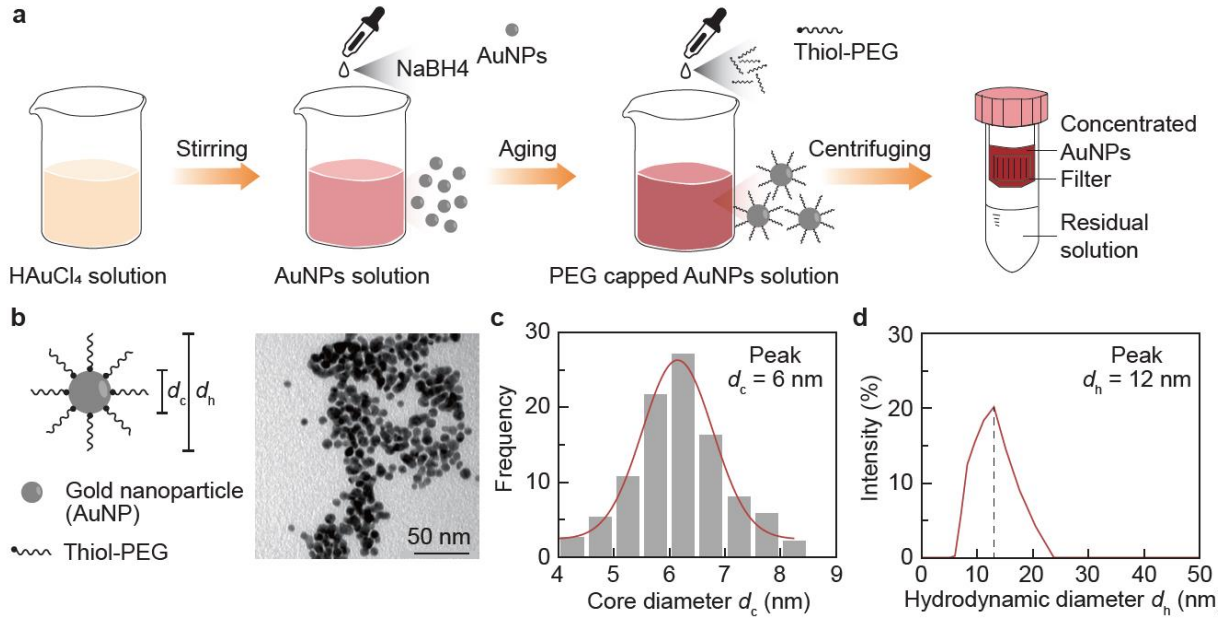

Synthesis and characterization of functionalized AuNPs with 6 nm core diameter. a, Schematic illustration of the procedure for synthesizing functionalized AuNPs with a 6 nm core diameter. **b,** Schematic illustration of the structure of functionalized AuNPs and its corresponding TEM image. **c**, Histogram of the AuNPs' core diameter d_c based on the TEM image. **d**, DLS spectrum to characterize the AuNPs' hydrodynamic diameter d_h.

Fig. S3.

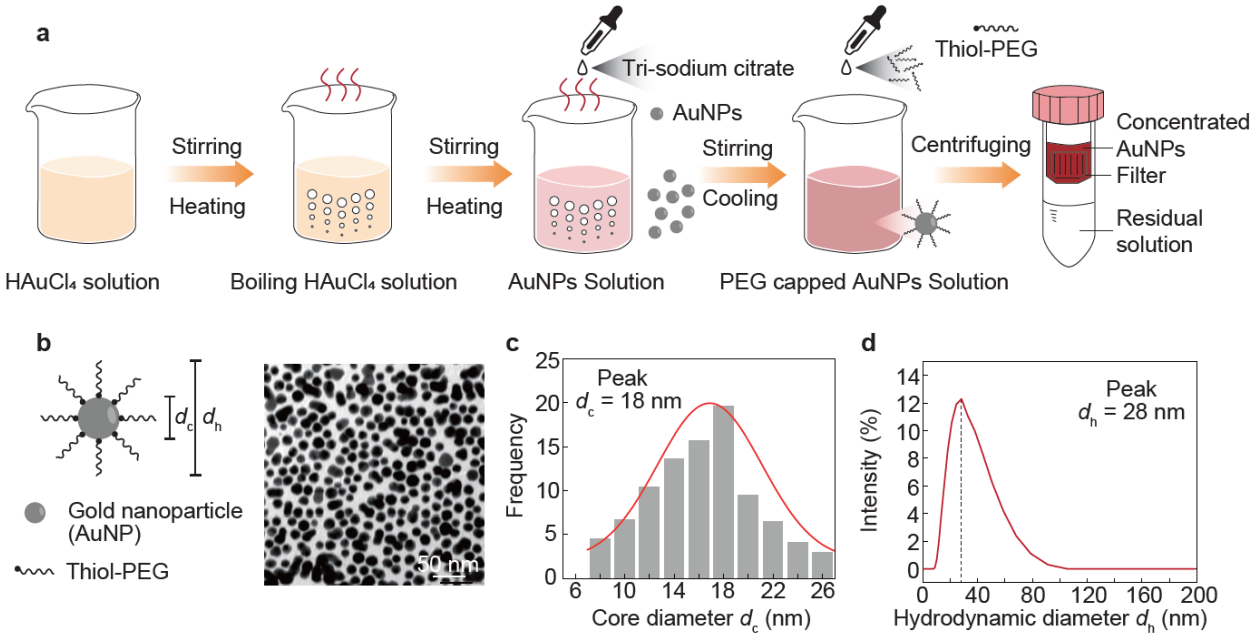

Synthesis and characterization of functionalized AuNPs with 18 nm core diameter. a, Schematic illustration of the procedure for synthesizing functionalized AuNPs with a 18 nm core diameter. **b,** Schematic illustration of the structure of functionalized AuNPs and its corresponding TEM image. **c**, Histogram of the AuNPs' core diameter d_c based on the TEM image. **d**, DLS spectrum to characterize the AuNPs' hydrodynamic diameter d_h.

Fig. S4.

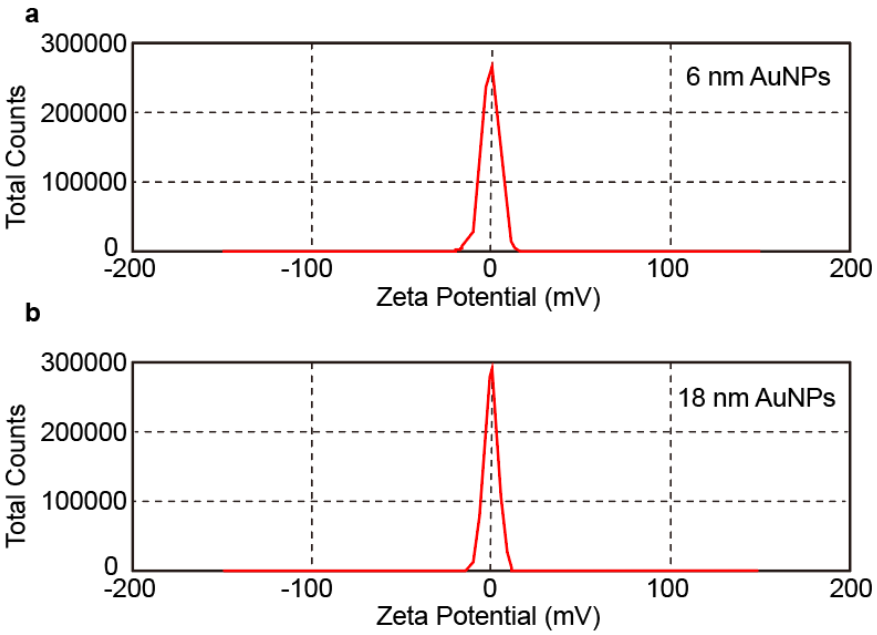

Zeta potential measurements of AuNPs. The zeta potentials of the synthesized AuNPs with **a**, 6 nm and **b**, 18 nm core diameter are nearly 0 mV, indicating their neutral surface electrokinetic potentials and inert surface charge characteristics.

Fig. S5.

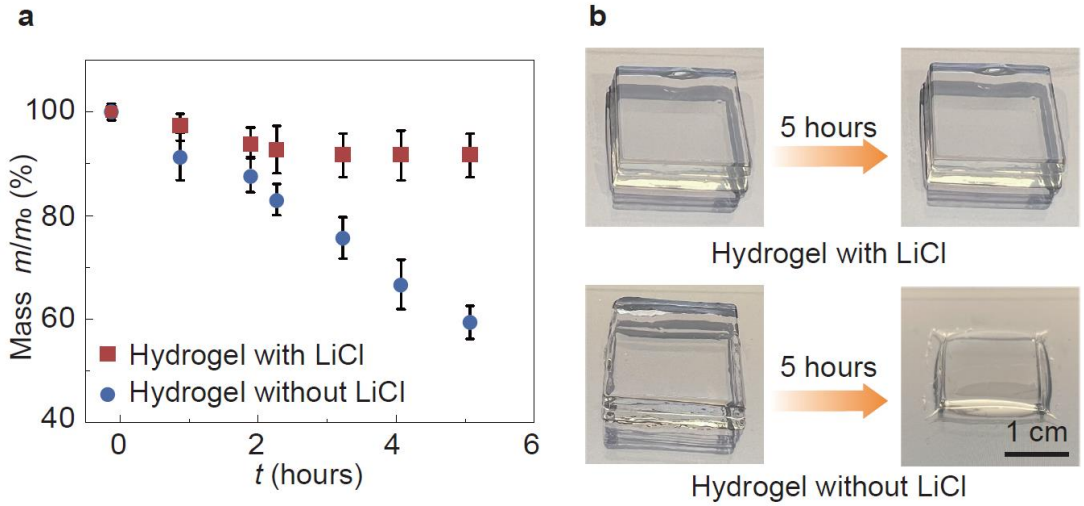

Characterization of water retention in hydrogels. a, Normalized mass m/m_0 versus time of hydrogels with and without LiCl exposed in an open environment, where m and m_0 are the measured masses of the hydrogel sample at time t and t = 0 hours, respectively. **b,** Images of the hydrogel samples with and without LiCl salt exposed in an open environment for 5 hours. The error bars in **a** represent the standard deviation from at least three independent tests.

Fig. S6.

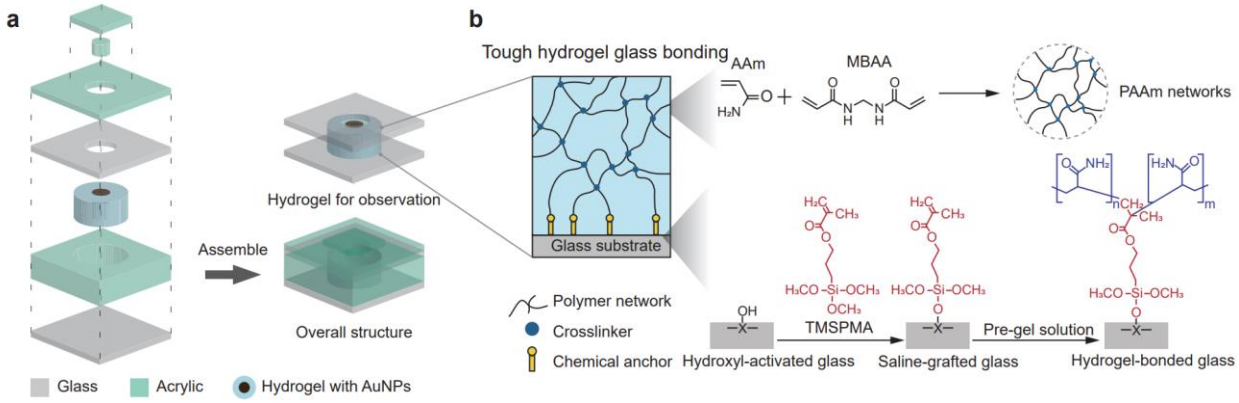

Device fabrication for the uniaxial mechano-diffusion characterization platform. a, Schematic illustrations of the assembly of an acrylic mold used to fabricate a cylindrical hydrogel sample confined between two glass substrates, containing a central reservoir designed to hold the AuNPs solution. **b**, the hydrogel sample is robustly bonded to glass via tough hydrogel glass bonding.

Fig. S7.

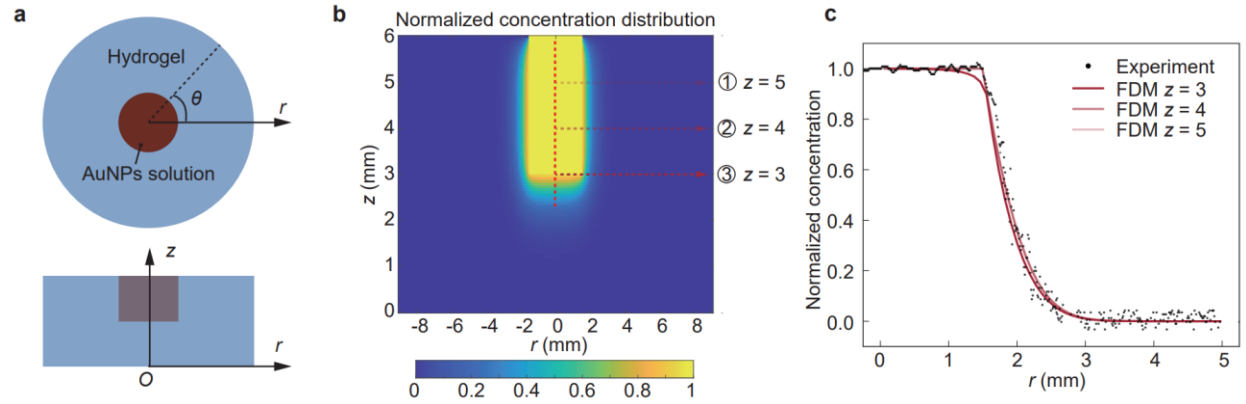

Extraction of AuNPs diffusivity in cylindrical hydrogels under tension or torsion by finite difference method (FDM). a, Schematic illustration of the cylindrical coordinate system for the hydrogel sample. **b,** Normalized concentration distribution of AuNPs diffusing in the *z*-*r* plane of the hydrogel sample, calculated using the finite difference method in MATLAB. **c,** Normalized concentration distribution of AuNPs as a function of *r* along radius direction at $z = 3$, $z = 4$, and $z = 5$. The solid dots denote the measured experimental results, and the solid lines denote the fitted simulation curves.

Fig. S8.

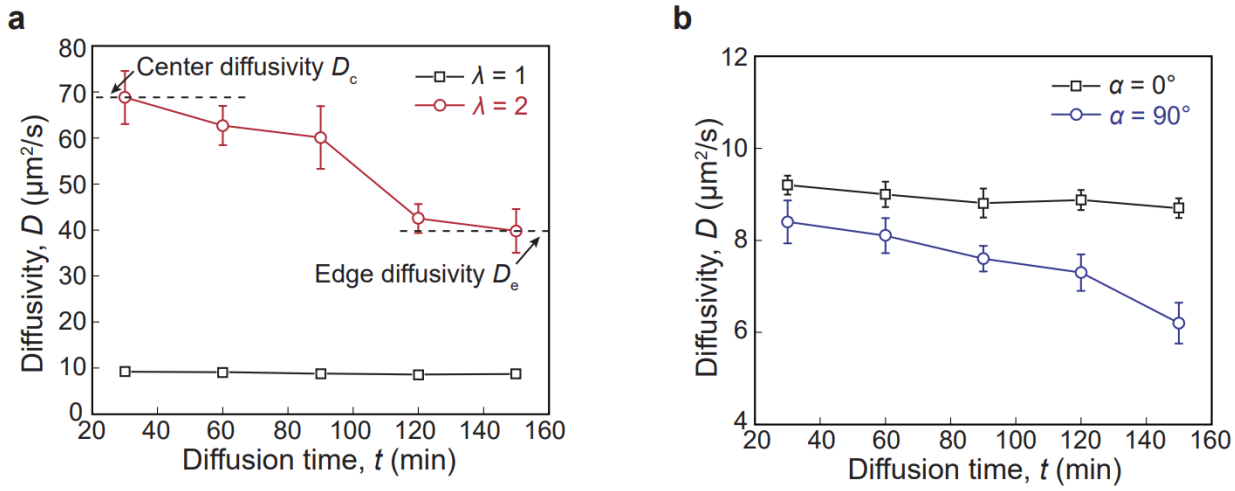

Extracted diffusivity of 6 nm AuNPs in undeformed, stretched, and twisted hydrogels. a, Comparison of the extracted diffusivity D as a function of diffusion time t in undeformed (λ = 1) and stretched (λ = 2) hydrogels. The short-term diffusivity corresponds to center diffusivity D_c, while the long-term diffusivity corresponds to center diffusivity D_e. **b**, Comparison of the extracted diffusivity D as a function of diffusion time t in undeformed (α = 0°) and twisted (α = 90°) hydrogels. The error bars in **a** and **b** represent the standard deviation from at least three independent tests.

Fig. S9.

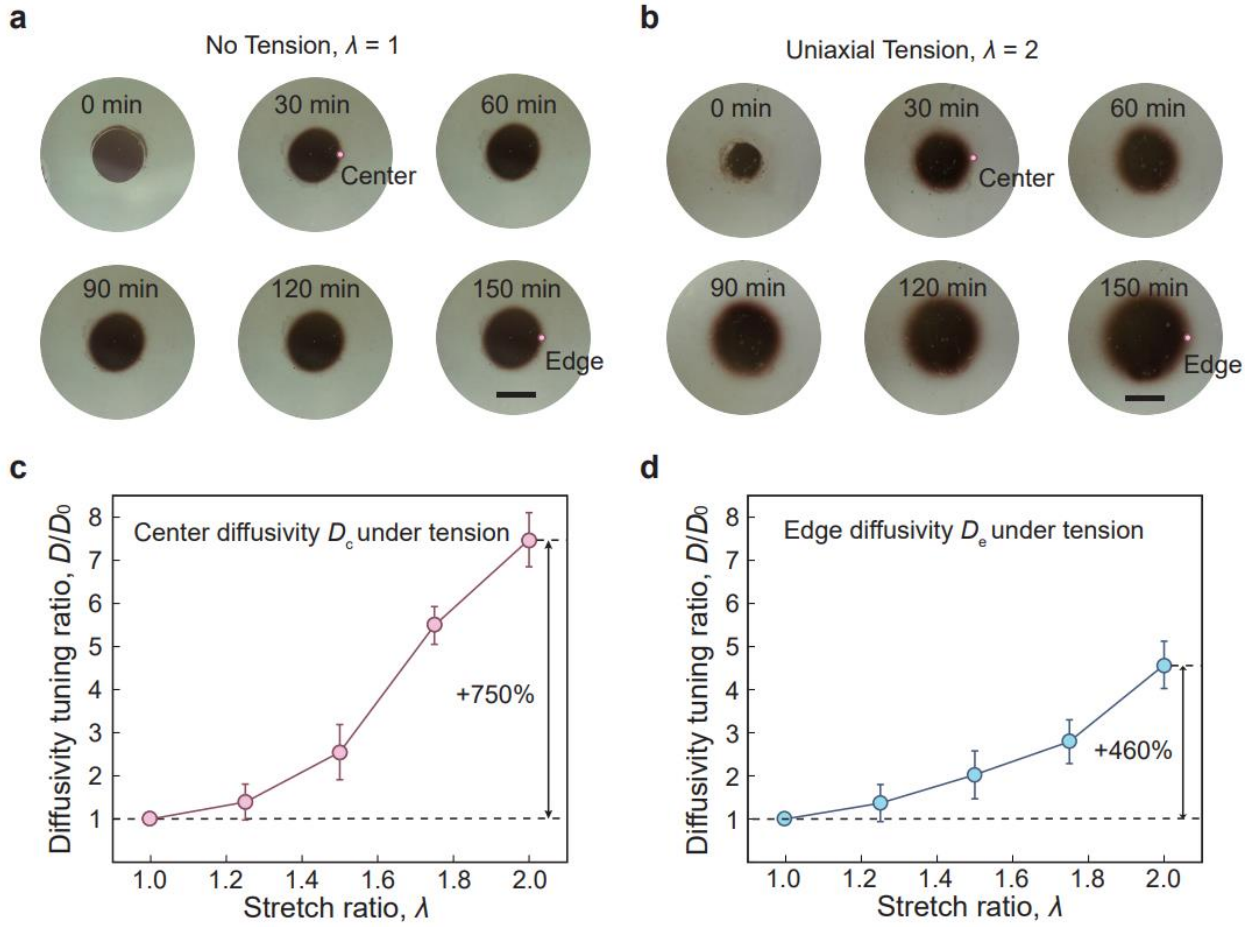

Effects of uniaxial tension on mechano-diffusion of 6 nm AuNPs in hydrogels. Optical images of 6 nm AuNPs diffusion **a**, in an unstretched hydrogel ($\lambda = 1$) and **b**, in a stretched hydrogel ($\lambda = 2$). The center diffusivity is defined as the diffusivity measured at 30 min, and the edge diffusivity is defined as the measured diffusivity at 150 min. **c**, Center diffusivity tuning ratio D_c/D_0 and **d**, edge diffusivity tuning ratio D_e/D_0 versus stretch ratio λ of 6 nm AuNPs in hydrogels under uniaxial tension.

Fig. S10.

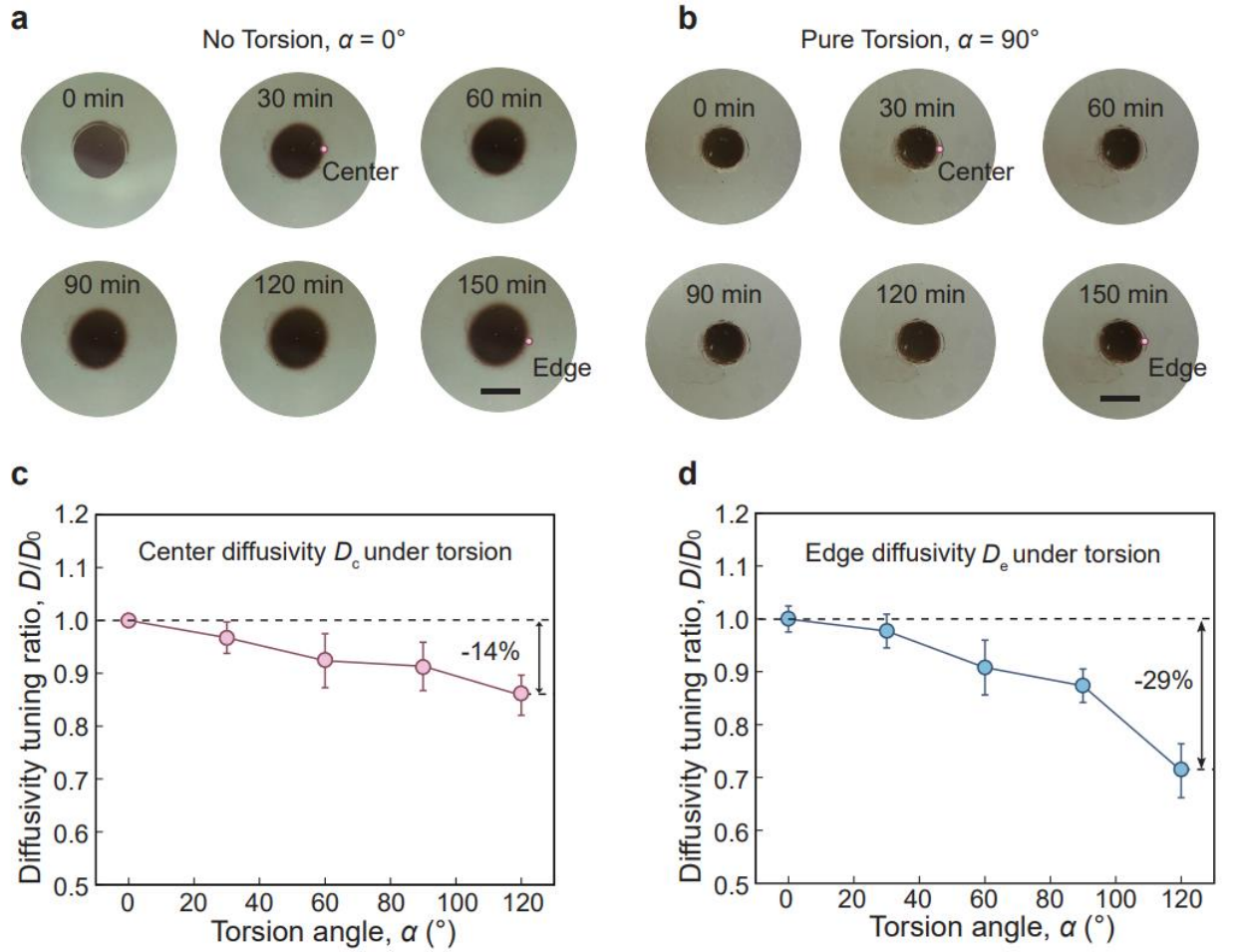

Effects of pure torsion on mechano-diffusion of 6 nm AuNPs in hydrogels. Optical images of 6 nm AuNPs diffusion **a**, in an untwisted hydrogel ($\alpha = 0°$) and **b**, in a twisted hydrogel ($\alpha = 90°$). The center diffusivity is defined as the diffusivity measured at 30 min, and the edge diffusivity is defined as the measured diffusivity at 150 min. **c**, Center diffusivity tuning ratio D_c/D_0 and **d**, edge diffusivity tuning ratio D_e/D_0 versus stretch ratio λ of 6 nm AuNPs in hydrogels under uniaxial tension.

Fig. S11.

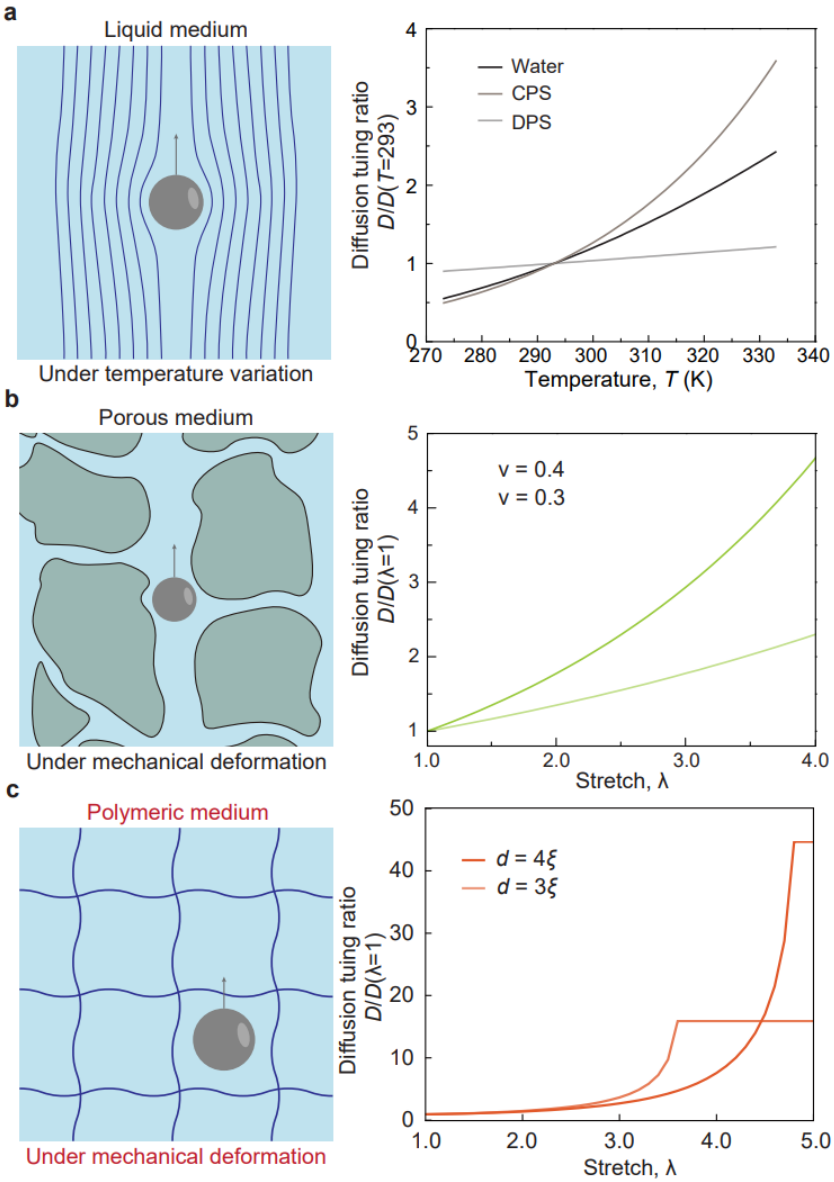

Particle diffusivity tuning ratios in various mediums. a, Particle diffusivity tuning ratio versus temperature T in water, concentrated polymer solution (CPS), diluted polymer solution (DPS). **b,** Particle diffusivity tuning ratio versus tensile stretch λ in the porous medium with various Poisson's ratio υ. **c,** Diffusivity tuning ratio $D/D(\lambda = 1)$ of particles with various size d versus tensile stretch λ in polymer networks with controlled mesh size ξ.

Fig. S12.

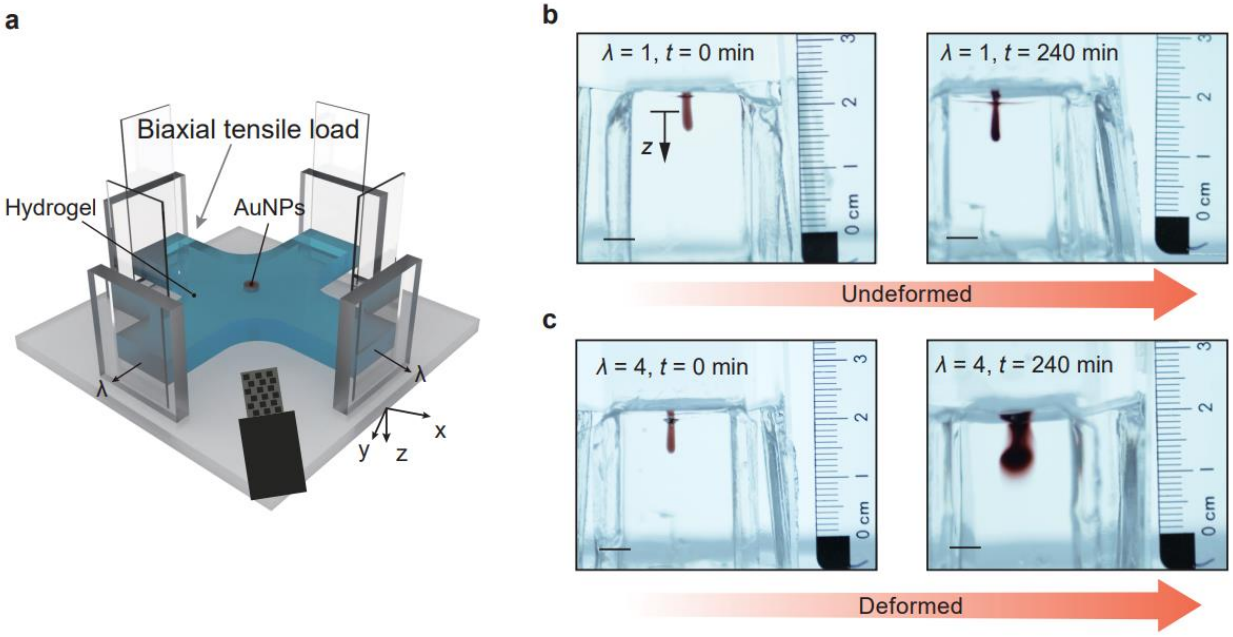

Biaxial mechano-diffusion characterizations. a, Schematic illustration of the experiment setup that includes an imaging system to measure the spatiotemporal diffusion profile of particles and a mechanical system to control and monitor the biaxial tensile deformation applied onto the hydrogel. **b, c,** Representative diffusion profiles of AuNPs in the hydrogel sample within 240 minutes. The scale bar in **b** is 5 mm.

Fig. S13.

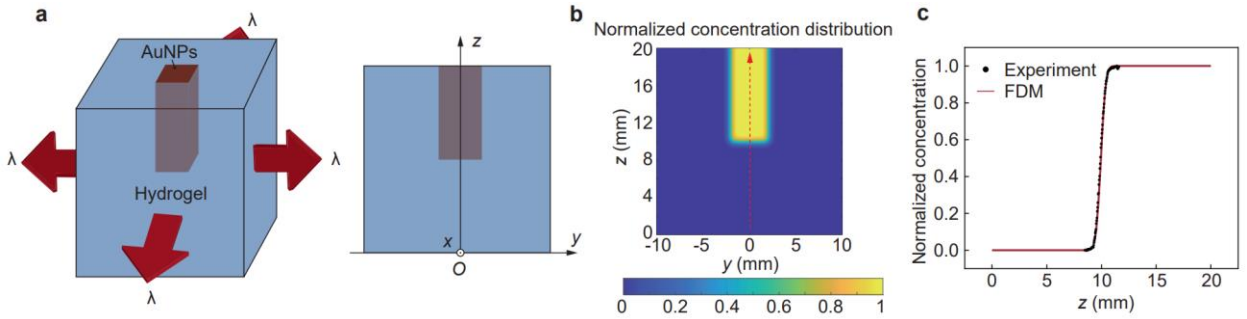

Extraction of AuNPs diffusivity in cubic hydrogels under biaxial tension by finite difference method (FDM). a, Schematic illustration of the cartesian coordinate system for the hydrogel sample. **b,** Normalized concentration distribution of AuNPs diffusing in the *z*-*y* plane of the hydrogel, calculated using the finite difference method in MATLAB. **c,** Normalized concentration distribution of AuNPs as a function of z at $x = y = 0$. The solid dots denote the measured experimental results, and the solid lines denote the fitted simulation curves.

Fig. S14.

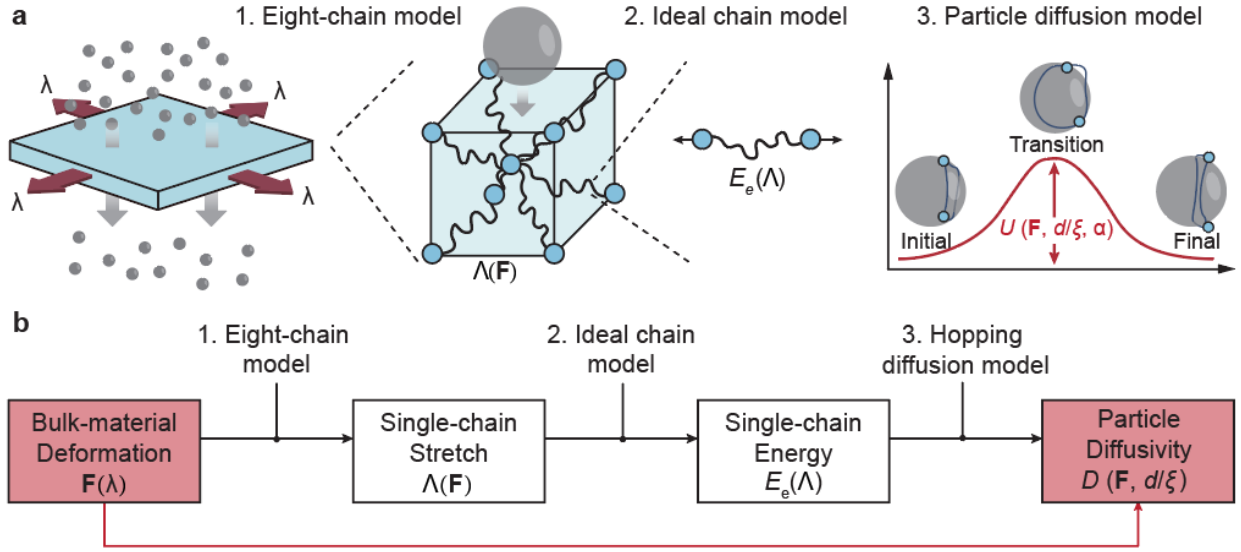

Theoretical framework of the mechano-diffusion theory. The mechano-transport theory **a,** integrates the eight-chain model, ideal-chain model, and particle diffusion model to **b,** establish the relationship between macroscopic large deformation of bulk materials $\mathbf{F}(\lambda)$ and microscale diffusion of particles $D(\mathbf{F}, d/\xi)$, where **F** is deformation gradient, d is particle diameter, and ξ is hydrogel mesh size.

Fig. S15.

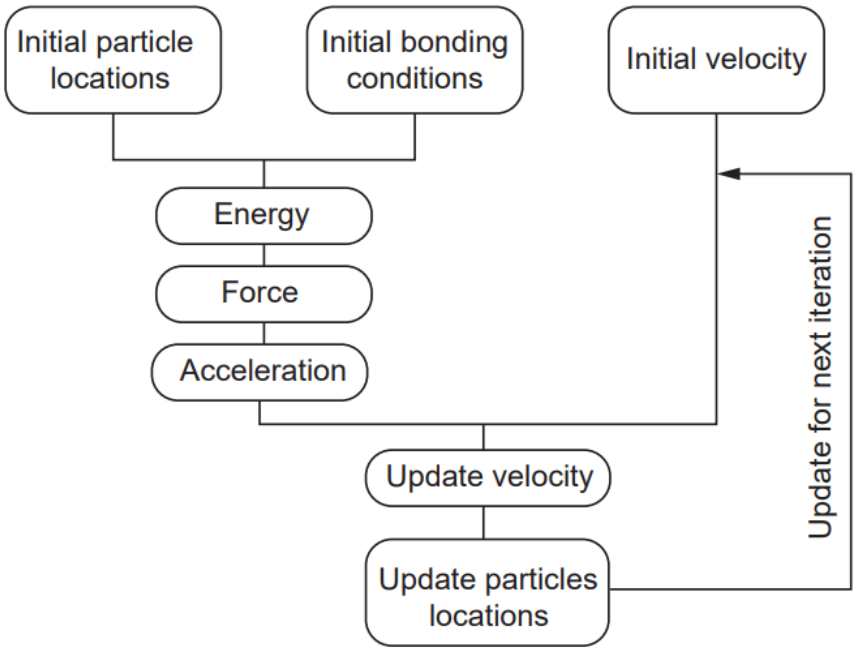

Flow chart of molecular dynamics simulation. Coarse-grained molecular dynamics using the software package LAMMPS.

Fig. S16.

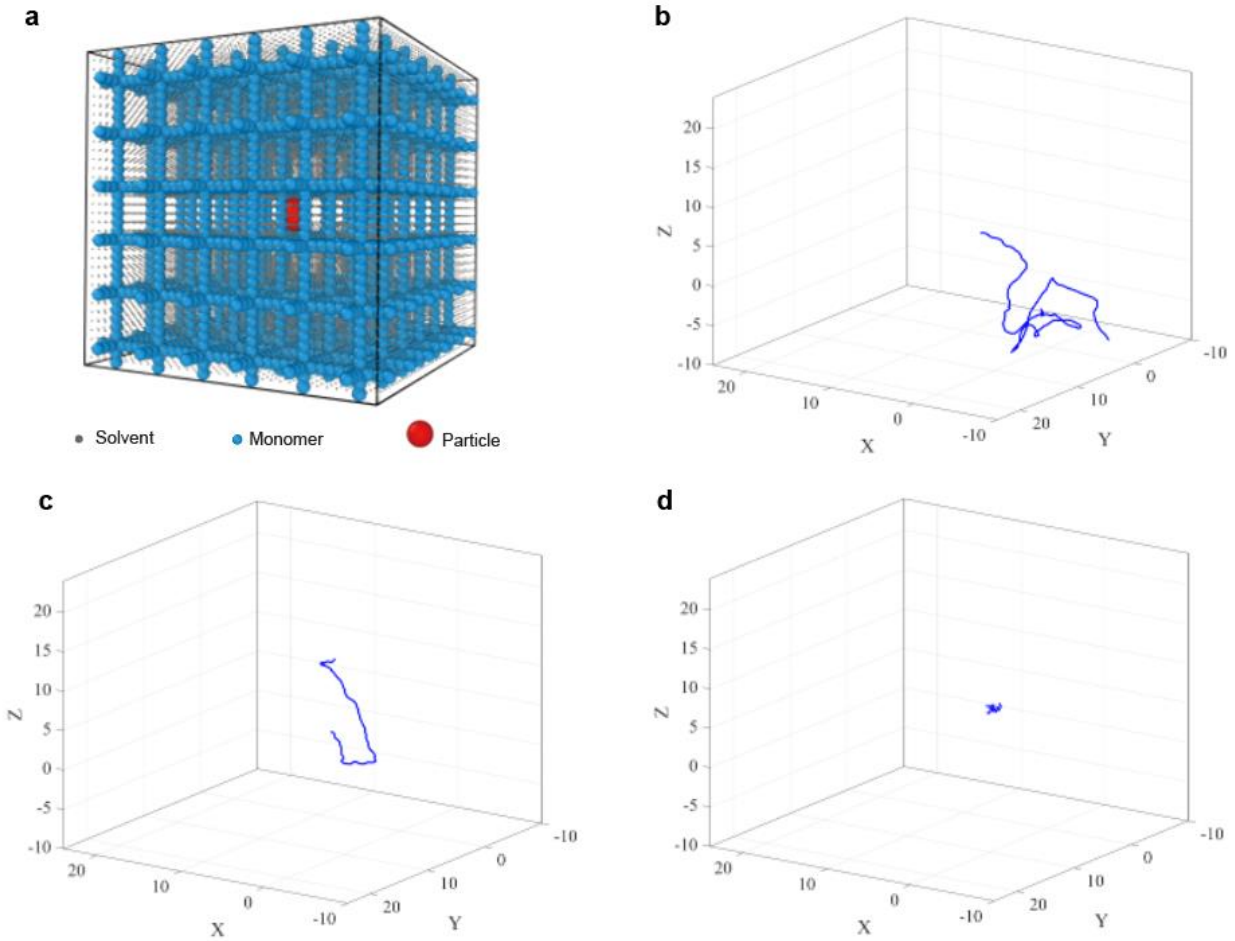

Simulated trajectory of particles with different diameters diffusing in undeformed polymer networks. a, The illustration of particle diffusion in undeformed polymer networks with mesh size ξ. **b,** the trajectory of the particle with diameter $d = 0.5\ \xi$. **b,** the trajectory of the particle with diameter $d = \xi$. **c,** the trajectory of the particle with diameter $d = 2\ \xi$.

Fig. S17.

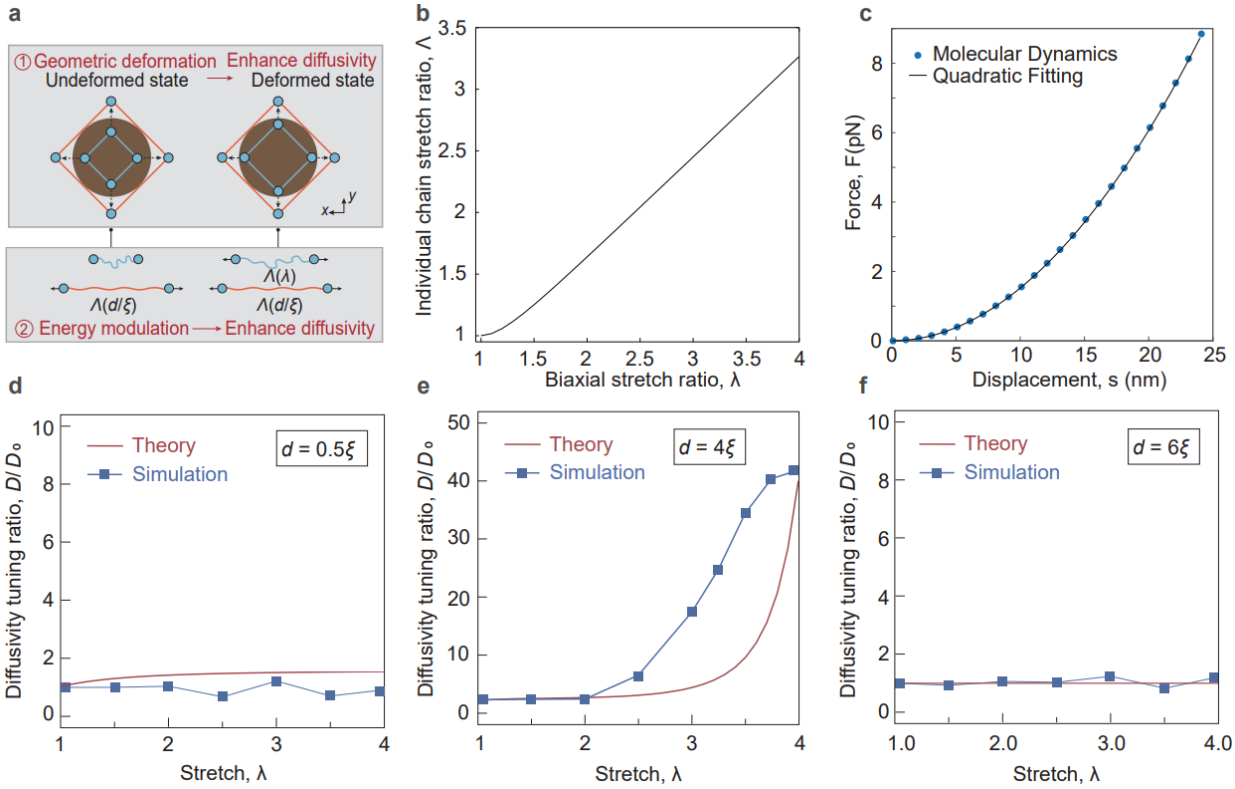

Comparison of particle diffusivity tuning in hydrogels under biaxial tension between theory and simulation. a, Schematic illustration of projected view of a particle passing through a cubic polymer network at undeformed and deformed state. Particle diffusivity is governed by the synergy of geometric deformation and energy modulation. **b**, Individual chain stretch ratio Λ as a function of biaxial stretch ratio λ following the eight-chain model. **c**, Force-displacement curve of an individual polymer chain. The discrete dots are from molecular dynamics results, fitted by a quadratic function as the solid line. **d**, Comparison of diffusivity tuning ratio D/D_0 versus stretch ratio λ for particles with diameters smaller than mesh size (e.g., $d = 0.5\xi$) between simulation and theory. **e,** Comparison of diffusivity tuning ratio D/D_0 versus stretch ratio λ for particles with diameters with diameters slightly larger than mesh size (e.g., $d = 4\xi$) between simulation and theory. **f**, Comparison of diffusivity tuning ratio D/D_0 versus stretch ratio λ for particles with diameters much larger than mesh size (e.g., $d = 6\xi$) between simulation and theory.

Fig. S18.

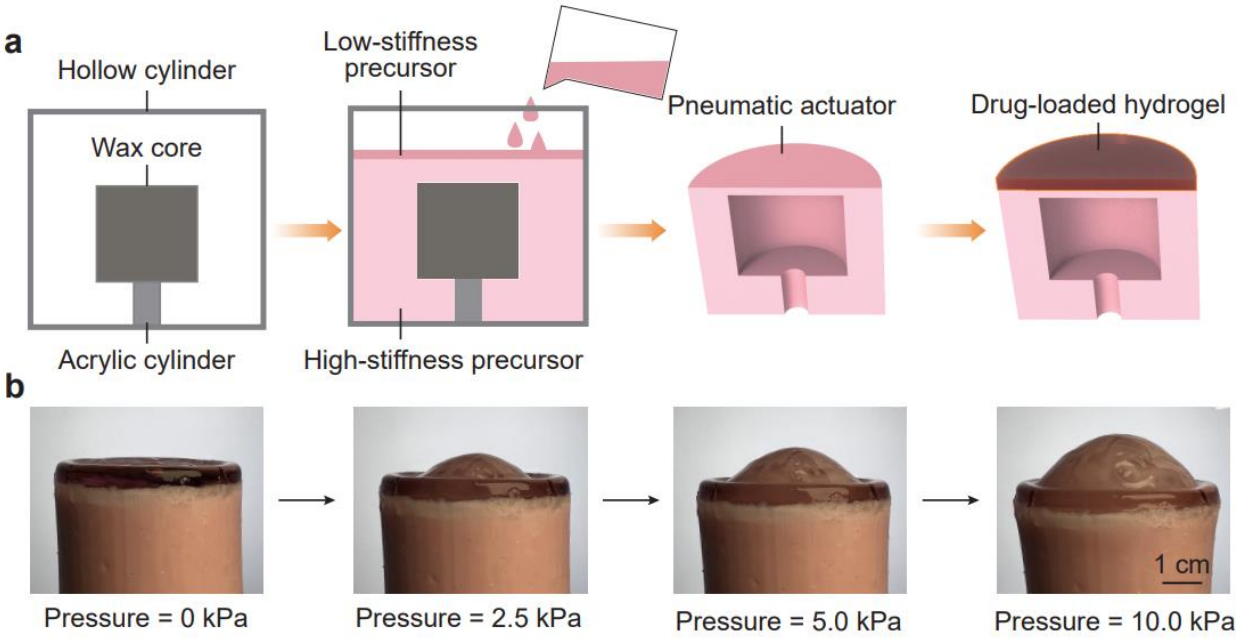

Fabrication of pressure-triggered drug delivery system. a, Fabrication process of the actuator, using lost-wax casting method with silicone rubber. **b**, Images of actuator under pressure of 0 kPa, 2.5 kPa, 5.0 kPa, and 10.0 kPa.

Fig. S19.

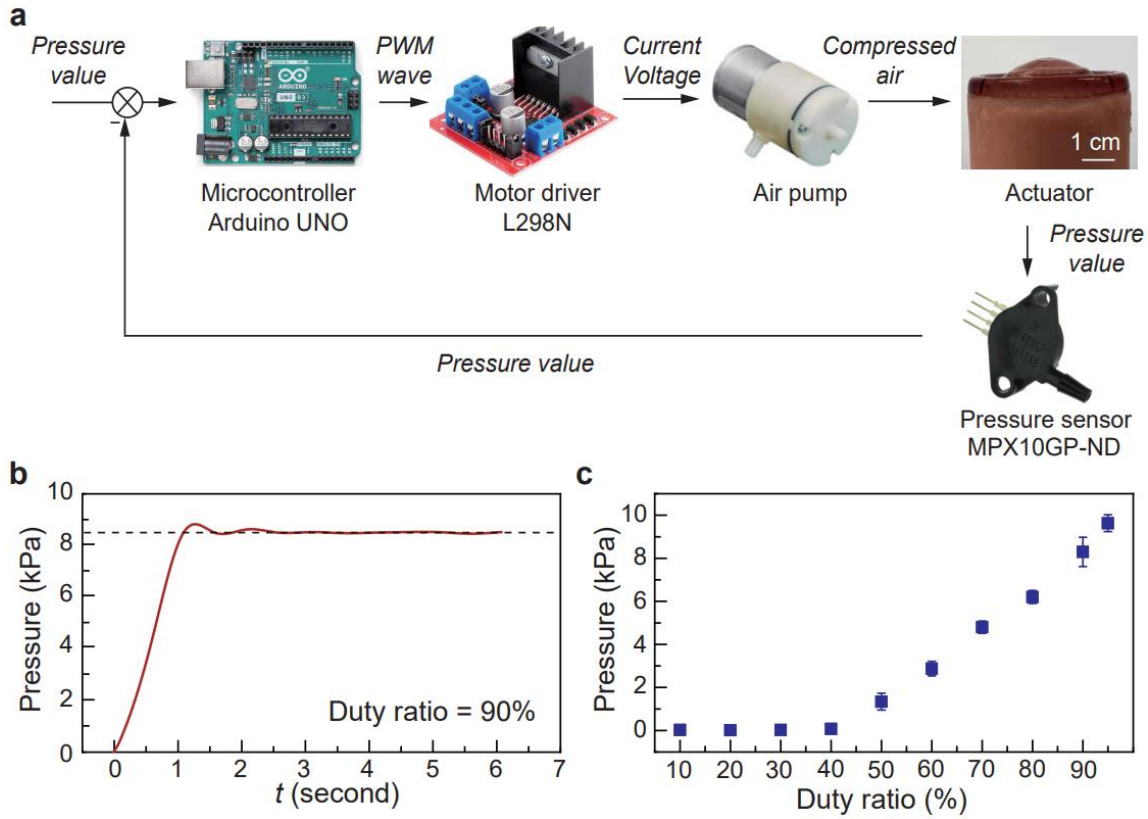

Air pressure control system of the actuator. a, The diagram of the control system, with a pressure value feedback loop. **b**, The dynamic performance of the pressure in the inflated actuator under the pulse width modulation (PWM) wave with 90% duty ratio. **c**, The relationship between the PWM wave duty ratio and the pressure in the actuator.

Fig. S20.

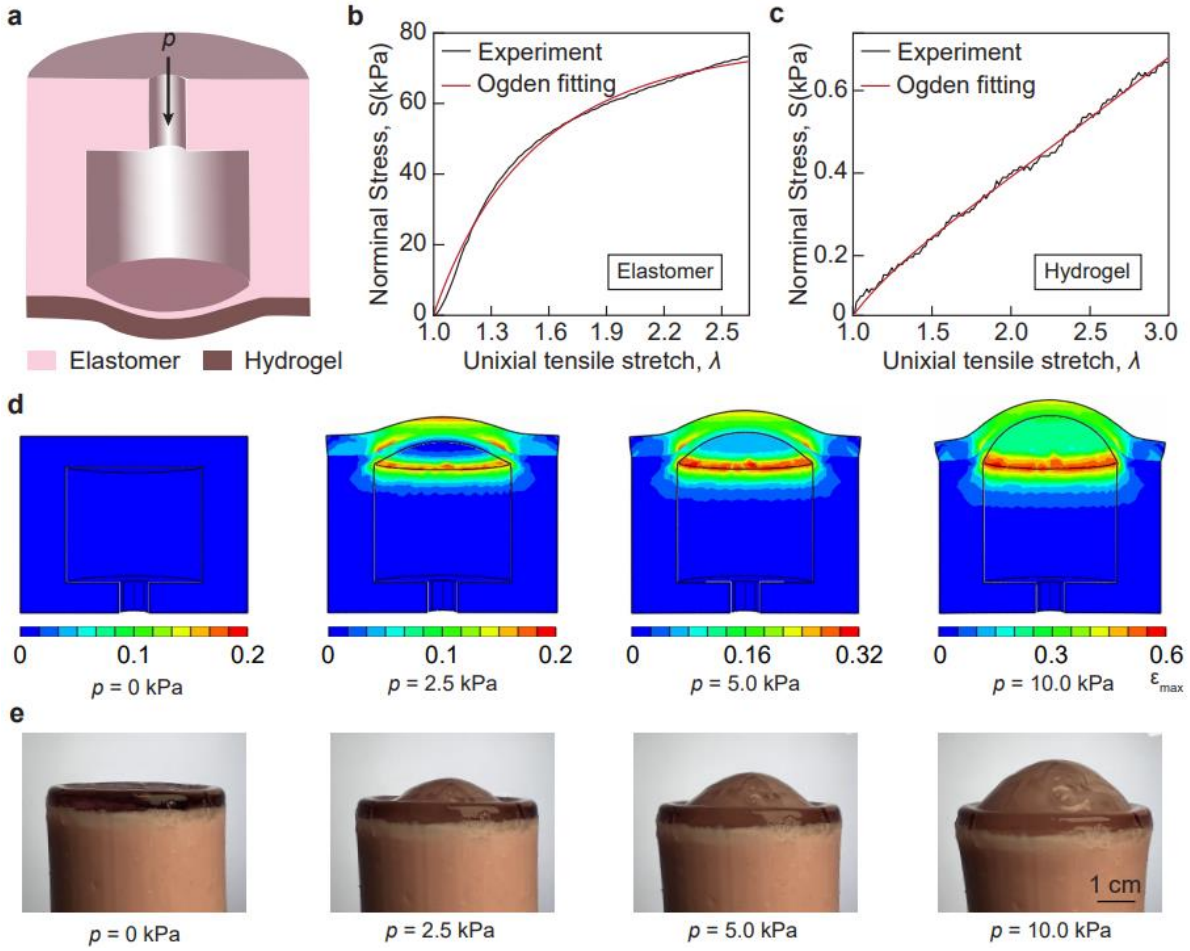

Programmable hydrogel deformation by controlled inflation pressure. a, pressure-triggered drug delivery system consists of an elastomeric actuator and a hydrogel membrane. **b**, Nominal stress versus stretch curve of the elastomer fitted by the Ogden model as the input for FEA simulation. **c**, Nominal stress versus stretch curve of the hydrogel fitted by the Ogden model as the input for FEA simulation. **d**, Snapshots of the stress distribution in the hydrogel membrane by inflating the elastomeric actuator with pressure of 0, 2.5, 5.0, and 10.0 kPa. $\boldsymbol{\varepsilon_{max}}$ is the maximum principal strain. **e**, Images of the deformed hydrogel membrane by inflating the elastomeric actuator with pressure of 0, 2.5, 5.0, and 10.0 kPa.

Table S1.

Summarized diffusivity tuning ratio and tuning time

Medium	Stimuli	Tuning ratio	Tuning time (min)	Reference
Water	Temperature	4.45	11.9	[14]
DPS	Temperature	1.34	16.7	[16]
CPS	Temperature	7.32	33	[15, 17, 18]
PS	Light	3.86	30	[28]
Water	Magnetic field	0.9987	0.1	[29]
Water	Electrical field	1.15	0.1	[30]
Tissue	Mechanical	0.45	2	[31]
This work	Mechanical	48	0.1	

Movie S1.
Impact of uniaxial tension on 6 nm AuNPs diffusion in hydrogels.

Movie S2.
Impact of pure torsion on 6 nm AuNPs diffusion in hydrogels.

Movie S3.
Impact of biaxial tension on 6 nm AuNPs diffusion in hydrogels.

Movie S4.
Impact of biaxial tension on particle diffusion in polymer networks.

Movie S5.
Programmable hydrogel deformation by controlled inflation pressure.

References

(1) Gole, A.; Murphy, C. J. Seed-mediated synthesis of gold nanorods: role of the size and nature of the seed. *Chemistry of Materials* **2004**, *16* (19), 3633-3640.

(2) Moncure, P. J.; Simon, Z. C.; Millstone, J. E.; Laaser, J. E. Relationship between gel mesh and particle size in determining nanoparticle diffusion in hydrogel nanocomposites. *The Journal of Physical Chemistry B* **2022**, *126* (22), 4132-4142.

(3) Murphy, A. G. a. C. J. Seed-Mediated Synthesis of Gold Nanorods: Role of the Size and Nature of the Seed. *Chemistry of Materials* **2004**, *16* (19), 3633–3640.

(4) Moncure, P. J.; Simon, Z. C.; Millstone, J. E.; Laaser, J. E. Relationship between Gel Mesh and Particle Size in Determining Nanoparticle Diffusion in Hydrogel Nanocomposites. *J Phys Chem B* **2022**, *126* (22), 4132-4142. DOI: 10.1021/acs.jpcb.2c00771.

(5) Kaszuba, M.; Corbett, J.; Watson, F. M.; Jones, A. High-concentration zeta potential measurements using light-scattering techniques. *Philosophical transactions of the royal society a: mathematical, physical and engineering sciences* **2010**, *368* (1927), 4439-4451.

(6) Schaefer, D. W. A unified model for the structure of polymers in semidilute solution. *Polymer* **1984**, *25* (3), 387-394.

(7) Yuk, H.; Zhang, T.; Lin, S.; Parada, G. A.; Zhao, X. Tough bonding of hydrogels to diverse non-porous surfaces. *Nature materials* **2016**, *15* (2), 190-196.

(8) Zhao, B.-R.; Li, B. Molecular simulation of hopping mechanisms of nanoparticles in regular cross-linked polymer networks. *The Journal of Chemical Physics* **2022**, *157* (10).

(9) Goodrich, C. P.; Brenner, M. P.; Ribbeck, K. Enhanced diffusion by binding to the crosslinks of a polymer gel. *Nature communications* **2018**, *9* (1), 4348.

(10) Mendez, K.; Whyte, W.; Freedman, B. R.; Fan, Y.; Varela, C. E.; Singh, M.; Cintron-Cruz, J. C.; Rothenbücher, S. E.; Li, J.; Mooney, D. J. Mechanoresponsive Drug Release from a Flexible, Tissue‐Adherent, Hybrid Hydrogel Actuator. *Advanced Materials* **2023**, 2303301.

(11) Parada, G. A.; Yuk, H.; Liu, X.; Hsieh, A. J.; Zhao, X. Impermeable robust hydrogels via hybrid lamination. *Advanced healthcare materials* **2017**, *6* (19), 1700520.

(12) Miller, C. C. The Stokes-Einstein law for diffusion in solution. *Proceedings of the Royal Society of London. Series A, Containing Papers of a Mathematical and Physical Character* **1924**, *106* (740), 724-749.

(13) Liu, Q.; Huang, S.; Suo, Z. Brownian Motion of Molecular Probes in Supercooled Liquids. *Phys Rev Lett* **2015**, *114* (22), 224301. DOI: 10.1103/PhysRevLett.114.224301.

(14) Poling, B. E.; Prausnitz, J. M.; O'connell, J. P. *Properties of gases and liquids*; McGraw-Hill Education, 2001.

(15) Dunstan, D. E. The viscosity-radius relationship for concentrated polymer solutions. *Scientific reports* **2019**, *9* (1), 543.

(16) Graessley, W. W. *Polymeric liquids & networks: structure and properties*; Garland Science, 2003.

(17) De Gennes, P.-G. *Scaling concepts in polymer physics*; Cornell university press, 1979.

(18) Flory, P. J. *Principles of polymer chemistry*; Cornell university press, 1953.

(19) Klepach, D.; Zohdi, T. Strain assisted diffusion: modeling and simulation of deformation-dependent diffusion in composite media. *Composites Part B: Engineering* **2014**, *56*, 413-423.

(20) Amsden, B. An obstruction-scaling model for diffusion in homogeneous hydrogels. *Macromolecules* **1999**, *32* (3), 874-879.

(21) Cai, L.-H.; Panyukov, S.; Rubinstein, M. Hopping diffusion of nanoparticles in polymer matrices. *Macromolecules* **2015**, *48* (3), 847-862.

(22) Ellen M. Arruda, M. C. B. A Three-dimensional Constitutive Model for the Large Stretch Behavior of Rubber Elastic Materials. *J. Mech. Phys. Solids* **1993**, *41*, 389-412.
(23) Rubinsten, M. *Polymer physics*; United States of America, 2003.
(24) Xu, Z.; Dai, X.; Bu, X.; Yang, Y.; Zhang, X.; Man, X.; Zhang, X.; Doi, M.; Yan, L.-T. Enhanced heterogeneous diffusion of nanoparticles in semiflexible networks. *ACS nano* **2021**, *15* (3), 4608-4616.
(25) Liu, J.; Lin, S. Strain-Engineered Particle Diffusion in Uniaxially Deformed Polymer Networks. *Journal of the Mechanics and Physics of Solids* **2024**, 105732.
(26) Arruda, E. M.; Boyce, M. C. A three-dimensional constitutive model for the large stretch behavior of rubber elastic materials. *Journal of the Mechanics and Physics of Solids* **1993**, *41* (2), 389-412.
(27) Kuhn, W.; Grün, F. Beziehungen zwischen elastischen Konstanten und Dehnungsdoppelbrechung hochelastischer Stoffe. *Kolloid-Zeitschrift* **1942**, *101*, 248-271.
(28) Moniruzzaman, M.; Bellerby, J. M.; Mai, N. The effect of light on the viscosity and molecular mass of nitrocellulose. *Polymer degradation and stability* **2011**, *96* (5), 929-935.
(29) Ghauri, S.; Ansari, M. Increase of water viscosity under the influence of magnetic field. *Journal of Applied Physics* **2006**, *100* (6).
(30) Zong, D.; Hu, H.; Duan, Y.; Sun, Y. Viscosity of water under electric field: Anisotropy induced by redistribution of hydrogen bonds. *The Journal of Physical Chemistry B* **2016**, *120* (21), 4818-4827.
(31) Schwartz, G.; Morejon, A.; Best, T. M.; Jackson, A. R.; Travascio, F. Strain-dependent diffusivity of small and large molecules in meniscus. *Journal of biomechanical engineering* **2022**, *144* (11), 111010.